Petroleum Science (2019) 16:874–889
https://doi.org/10.1007/s12182-018-0294-2

ORIGINAL PAPER

A compositional model for CO_2 flooding including CO_2 equilibria between water and oil using the Peng–Robinson equation of state with the Wong–Sandler mixing rule

Zhong-Lin Yang[1,2,3] · Hai-Yang Yu[1,2,3] · Zhe-Wei Chen[1,2,3] · Shi-Qing Cheng[1,2,3] · Jian-Zheng Su[1,2]

Received: 10 July 2018 / Published online: 10 January 2019

Abstract

This paper presents a three-dimensional, three-phase compositional model considering CO_2 phase equilibrium between water and oil. In this model, CO_2 is mutually soluble in aqueous and hydrocarbon phases, while other components, except water, exist in hydrocarbon phase. The Peng–Robinson (PR) equation of state and the Wong–Sandler mixing rule with non-random two-liquid parameters are used to calculate CO_2 fugacity in the aqueous phase. One-dimensional and three-dimensional CO_2 flooding examples show that a significant amount of injected CO_2 is dissolved in water. Our simulation shows 7% of injected CO_2 can be dissolved in the aqueous phase, which delays oil recovery by 4%. The gas rate predicted by the model is smaller than the conventional model as long as water is undersaturated by CO_2, which can be considered as "lost" in the aqueous phase. The model also predicts that the delayed oil can be recovered after the gas breakthrough, indicating that delayed oil is hard to recover in field applications. A three-dimensional example reveals that a highly stratified reservoir causes uneven displacement and serious CO_2 breakthrough. If mobility control measures like water alternating gas are undertaken, the solubility effects will be more pronounced than this example.

Keywords CO_2 flooding · Wong–Sandler mixing rule · Equation of state · Numerical simulation · CO_2 solubility

List of symbols

$\underline{A}$	Molar Helmholtz free energy
A	Area of surface between two grid blocks
B	Second virial coefficient
B_w^*	Formation volume factor of a brine without solution gas
B_w	FVF of a brine at saturated condition
F	Arbitrary function
L	Distance between two grid blocks
K	Permeability, mD
K_r	Relative permeability
K_{rw}	Relative permeability of water
K_{rgcw}	Relative permeability of gas at connate water saturation
K_{rocw}	Relative permeability of oil at connate water saturation
Q	Quadratic sum of second virial coefficients
R_{sw}	Gas solubility in the aqueous phase (scf/STB)
R	Gas constant (J K^{-1} mol^{-1})
P	Pressure (Pa)
S_o, S_g, S_w	Oil, gas, and water saturation, fraction
S_{wc}	Connate water saturation
S_{org}	Residual oil saturation to gas
S_{gc}	Critical gas saturaion
S_{gr}	Residual gas saturation
T	Transmissibility (mD m)
T_F	Temperature in Fahrenheit (°F)
T_{cels}	Temperature in Celsius (°C)
$\underline{V}$	Molar volume (m^3/mol)
a	Equation of state "energy" parameter

Handling editor: Wen-Dong Wang

Edited by Yan-Hua Sun

✉ Hai-Yang Yu
haiyangyu.cup@139.com

[1] State Key Laboratory of Shale Oil and Gas Enrichment Mechanisms and Effective Development, Beijing 100083, China

[2] State Energy Center for Shale Oil Research and Development, Beijing 100083, China

[3] School of Petroleum Engineering, China University of Petroleum, Beijing 102249, China

b	Equation of state "excluded volume" parameter
c_{w}^{*}	Compressibility of a brine without solution gas (psi^{-1})
c_{w}	Compressibility of a brine without solution gas (psi^{-1})
f_i	Fugacity of component i at zero salinity (Pa)
$f_{i,\mathrm{s}}$	Fugacity of component i in brine (salt solution) (Pa)
$f_{i,\mathrm{o}}$	Fugacity of component i in oil (Pa)
$f_{i,\mathrm{g}}$	Fugacity of component i in gas (Pa)
$f_{\mathrm{CO_2,o}}$	CO_2 fugacity in oil (Pa)
$f_{\mathrm{CO_2,g}}$	CO_2 fugacity in gas (Pa)
$f_{\mathrm{CO_2,w}}$	CO_2 fugacity in water (Pa)
g	Local composition factor for the NRTL model
k_{ij}	Binary interaction coefficient between components i and j
$k_{i\mathrm{s}}$	Salting-out coefficient for component i
$k_{\mathrm{CO_2,s}}$	Salting-out coefficient for component CO_2
m_{s}	Molality of the dissolved salt (mol/kg)
q_{w}, q_i	Water well rate and hydrocarbon component i well rate (mol/s)
$p_{\mathrm{c,ow}}$, $p_{\mathrm{c,go}}$	Oil–water and gas–oil capillary pressure, respectively (Pa)
p_{o}, p_{g}, p_{w}	Oil, gas, and water pressure, respectively (Pa)
w_{s}	Weight fraction of NaCl (fraction)
x_i, y_i	Mole fraction of component i in the oil and gas phases, fraction
$x_{\mathrm{w\,CO_2}}$	Mole fraction of CO_2 in the aqueous phase (fraction)
$x_{\mathrm{wH_2O}}$	Mole fraction of H_2O in the aqueous phase (fraction)
Δ	Difference operator
$\delta_{i,\mathrm{CO_2}}$	Kronecker delta
λ_{o}, λ_{g}, λ_{w}	Oil, gas, and water mobilities (1/cP)
$\boldsymbol{\Phi}_{\mathrm{o}}$, $\boldsymbol{\Phi}_{\mathrm{g}}$, $\boldsymbol{\Phi}_{\mathrm{w}}$	Oil, gas, and water potentials (Pa)
μ	Viscosity (cP)
α	NRTL model parameter
τ	NRTL model binary interaction parameter
φ	Fugacity coefficient
γ	Activity coefficient
ϕ	Porosity (fraction)
o, g, w	Oil, gas, and aqueous phases, respectively
i	Component index
p	Phase (o, g, w)
*	Simulation results of the conventional model

1 Introduction

Modeling transient flow of reservoir fluids with large variations in compositions requires a compositional model (Ju et al. 2012; Cho et al. 2018). It has become mainstream to simulate multiphase flow such as miscible gas injection and depletion of volatile oil/gas-condensate reservoirs. In most published models, for example, Fussell and Fussell (1979), Coats (1980), Young and Stephenson (1983), and Chien et al. (1985), water is treated as an independent component where hydrocarbon components are not allowed to dissolve. This assumption is appropriate for gas injection where the components are hard to dissolve in the aqueous phase. CO_2 flooding, however, is not suited for this assumption because CO_2 solubility in water is much higher than that of hydrocarbons, whose effect cannot be neglected in the simulation process. This is especially true when CO_2 is injected into previously waterflooded reservoirs or into tight oil reservoirs where connate water saturation is up to 50%. Enick and Klara (1992) and Chang et al. (1998) demonstrated that the CO_2 dissolved in the formation brine accounts for a significant fraction of the total amount of CO_2 injected into the reservoir and the CO_2 solubility has a substantially adverse effect on the ultimate recovery. Therefore, a reliable and efficient compositional simulator including CO_2 solubility in water is needed to achieve more accurate simulation results.

The first challenge to develop such a simulator is how to model the phase behavior in the aqueous phase. Many researchers have experimentally studied the binary CO_2/water system (King et al. 1992; Valtz et al. 2004; Guo et al. 2014) and proposed numerous approaches to model the behavior (Pedersen et al. 2001; Spycher et al. 2003). The traditional fugacity approach that uses the cubic equation of state (EOS) with the van der Waals (vdW) mixing rule correlates the phase behavior of hydrocarbon mixtures accurately as long as appropriate binary interaction parameters are selected (Zhao and Lvov 2016). However, it is insufficient to obtain reliable results for a mixture containing strongly polar components like water. Over the past three decades, much effort has been devoted to modifying or replacing the vdW one-fluid mixing rule for the challenging vapor–liquid equilibrium calculation (Zhao and Lvov 2016).

Among the modern approaches presented in the literature, a method of the type "EOS + excess Gibbs free energy" (EOS/G^{ex}) is the most adequate for modeling mixtures with highly asymmetric components. Mixing rules proposed by Huron and Vidal (1979) and Wong and Sandler (1992), belonging to the EOS/G^{ex} type, have been extensively used and applied to highly challenging phase equilibria. Compared with the Huron–Vidal mixing rule,

the Wong–Sandler (WS) mixing rule satisfies the quadratic mole fraction dependence of the second virial coefficient and predicts the same excess Helmholtz energy at infinite pressure as a function of composition as that obtained from a selected activity coefficient model (Zhao and Lvov 2016). Many studies show the combination of WS mixing rule with non-random, two-liquid (NRTL) parameters gives the best results for water-containing polar mixtures compared to other mixing rules coupling cubic EOS (Valderrama 2003). Jaubert and Mutelet (2004) and Jaubert et al. (2010) proposed a group contribution-based thermodynamic model (PPR78 EOS) which combines, at a constant packing fraction, the Peng–Robinson (PR) EOS and a van Laar-type G^{ex} model. Their article demonstrates that using classical mixing rules, the PPR78 model is able to estimate the temperature-dependent K_{ij} (the binary interacting coefficient) for any mixtures containing alkanes, aromatics, naphthenes, CO_2, N_2, H_2S, and mercaptans. The innovative part of their work is to establish a predictive model that is able to estimate the interactions from mere knowledge of the structure of molecules within the petroleum blend. They proved that the PPR78 model can reliably predict the vapor–liquid equilibrium (VLE) of very asymmetric systems, which points out a new trend to predict the phase behavior of polar–nonpolar systems.

In addition to the EOS approach, Li and Nghiem (1986) used Henry's law to estimate CO_2 solubility in distilled water and used the scaled particle theory to take into account the presence of salt in the aqueous phase. The fugacity coefficients of light components that are considered soluble in the aqueous phase (e.g., methane, ethane, propane, and CO_2) can be derived from Henry's constant, and for hydrocarbon phase, they are calculated by the conventional cubic EOS with the vdW mixing rule. A time-consuming three-phase flash calculation is accomplished to obtain the phase equilibrium of the water–oil–gas system. Enick and Klara (1990) used the Krichevsky–llinskaya equation to correlate the solubility of CO_2 in water, and the decreased solubility of CO_2 in brine was accounted for empirically by a single factor correlated with the weight percent of dissolved solids. Chang et al. (1998) also proposed an empirical correlation for the solubility of CO_2 in distilled water as a function of temperature. The solubility in distilled water can be adjusted further for the effect of salinity to obtain the solubility of CO_2 in brine. Apart from this simple correlation, Chang et al. proposed an isothermal, three-dimensional composition model with both fully implicit and implicit pressure explicit saturation formulations. The innovative point of their work is that CO_2 fugacity coefficients in the aqueous phase are computed internally from the correlation and the equal-fugacity constraint of CO_2 for aqueous and hydrocarbon phases is introduced to solve the aqueous composition. Yan and Stenby (2009, 2010) used the PR EOS modified by Søreide and Whitson to describe the phase equilibrium between CO_2 and brine. A one-dimensional slim tube simulator combined with a multiphase flash subroutine was proposed to model CO_2 flooding considering the influence of CO_2 solubility, where the aqueous phase was treated as an inert phase or only dissolving CO_2.

To consider the CO_2 solubility in water, the existing reservoir compositional simulation is either with the aid of Henry's law or with empirical correlations. Although the EOS/G^{ex} approach is used widely in predicting the fluid phase equilibrium of polar components in process design, this model has never been integrated into reservoir simulation to fulfill the challenging simulation of CO_2 flooding including CO_2 equilibria between water and oil. In this work, we validate the EOS/G^{ex} model by reproducing the experimental PVT data of the binary CO_2–H_2O system and then provide formulations about how to integrate the EOS/G^{ex} model into the reservoir compositional simulation. Finally, we compare the simulation performance of our model with the existing compositional model. The simulation results of this study help to improve the accuracy of the numerical simulation of the oil recovery process involving CO_2, which will, in turn, improve the quality of the reservoir performance prediction and the reliability of the economic calculations.

2 General description of the model

The simulator described here is an isothermal, three-dimensional compositional model. Fully implicit formulations are presented which are able to treat water, oil, and gas flow through reservoirs of heterogeneous permeability and porosity. It is designed to model the compositional flow process considering the CO_2 phase equilibrium between the aqueous phase and the hydrocarbon phase. This simulator does not model the three-hydrocarbon-phase phenomenon that has been observed for some CO_2/hydrocarbon systems.

The model consists of mass balance equations for water and n_c hydrocarbon components and associated constraint equations. Oil- and gas-phase densities and fugacities are calculated from the PR EOS, while the CO_2 fugacity in the aqueous phase, adjusted by a salting-out coefficient, is calculated by PR EOS with WS mixing rule (we denote the model proposed in this paper as the PR–WS model). Oil and gas viscosities are calculated by the Lohrenz et al. (1964) method. The fluid flow is simulated with Darcy's law, incorporating viscous, gravitational, and capillary forces.

Formulation assumptions are an instantaneous equilibrium between gas and oil phases in each grid, and only CO_2 is considered mutually soluble in water and oil. One reason for this is that the CO_2 solubility in water is significantly larger than other hydrocarbon components. Another reason is that when large quantities of CO_2 are injected during CO_2

flooding, it becomes the dominant component dissolved in water compared to other relatively highly soluble constituents like H_2S. This assumption is able to simplify the phase behavior calculation in the aqueous phase and reduce computation time greatly. Moreover, an equal-fugacity constraint of CO_2 between water and oil is used to characterize partitioning CO_2 in water and oil.

3 The PR–WS composition model

3.1 Reservoir model equations

Mass balance-type equations are used to describe the multicomponent multiphase flow in porous media. These equations can be divided into three parts (Young and Stephenson 1983): (1) mass balance equations describing component flow, (2) phase equilibrium relationships, and (3) constraint equations that require the phase saturation to sum to unity and the mole fraction in each phase to sum to unity.

For simplicity of development, the specific model assumptions are summarized as follows: (1) The dispersion and gravity forces are neglected, (2) only CO_2 is considered mutually soluble in water and oil, and water has no mass exchange with the hydrocarbon, (3) the effect of gas (mainly CO_2) on the aqueous viscosity is not considered because it was found to be very small, and (4) aqueous phase properties, such as the formation volume factor, water compressibility, and water viscosity, are calculated by empirical correlations.

With these assumptions,

(1) The $n_c + 1$ mass balance equations:

$$F_i = \frac{\partial}{\partial t}\left[V\phi(S_o\rho_o x_i + S_g\rho_g y_i + S_w\rho_w x_{w\,CO_2}\delta_{i,CO_2})\right] - \Delta\left[T(\lambda_o\rho_o x_i\Delta\Phi_o + \lambda_g\rho_g y_i\Delta\Phi_g + \lambda_w\rho_w x_{w\,CO_2}\delta_{i,CO_2}\Delta\Phi_w)\right] + q_i = 0 \qquad (i = 1, 2, \ldots, n_c) \tag{1}$$

$$F_w = \frac{\partial}{\partial t}\left[V\phi S_w\rho_w x_{wH_2O}\right] - \Delta\left[T\left(\lambda_w\rho_w x_{wH_2O}\Delta\Phi_w\right)\right] + q_w = 0, \tag{2}$$

δ_{i,CO_2} is the Kronecker delta, where δ_{i,CO_2}=1, if component i is CO_2; otherwise, δ_{i,CO_2}= 0.

Transmissibility is calculated by

$$T = \frac{KA}{\Delta L}. \tag{3}$$

Phase mobility is determined by

$$\lambda_p = \frac{K_{rp}}{\mu_p} \quad p = w, o, g. \tag{4}$$

Phase potential difference between grid blocks i and j is defined as

$$\Delta\Phi_{p,i,j} = \Delta\Phi_{p,j} - \Delta\Phi_{p,i} = p_{p,j} - p_{p,i}. \tag{5}$$

(2) The $n_c + 1$ fugacity equations (for a three-phase block)

$$F_{eh} = f_{i,o} - f_{i,g} = 0 \quad i = 1, 2, \ldots, n_c. \tag{6}$$

$$F_{ew} = f_{CO_2,w} - f_{CO_2,h} = 0 \quad h = o, g. \tag{7}$$

where h is one of the hydrocarbon phases (o or g), expressing that oil- and gas-phase fugacities must be equal for each hydrocarbon component, and CO_2 fugacities in hydrocarbon phase and aqueous phase must be equal too.

(3) Six constraint equations

Capillary pressure constraints:

$$F_{pcow} = p_{c,ow} - (p_o - p_w) = 0. \tag{8}$$

$$F_{pcgo} = p_{c,go} - (p_g - p_o) = 0. \tag{9}$$

Saturation or volume constraint:

$$F_s = S_o + S_g + S_w. \tag{10}$$

Component mole fraction constraints:

$$F_{po} = \sum_{i=1}^{n_c} x_i - 1 = 0. \tag{11}$$

$$F_{pg} = \sum_{i=1}^{n_c} y_i - 1 = 0. \tag{12}$$

$$F_{pw} = x_{wH_2O} + x_{w\,CO_2} - 1 = 0. \tag{13}$$

The equations and unknown variables are listed in Table 1. Linear constraint equations (F_{pcow}, F_{pcgo}, F_s, F_{po}, F_{pg}, and F_{pw}) are used to remove two pressures, one saturation, and three-component mole fractions. Finally, only $2n_c + 2$ nonlinear equations and variables are left, which is the full set of equations and variables. This full set can be further divided into primary and secondary equations and variables. Gaussian elimination is used to solve for the $n_c + 1$ unknowns of $y_i, i = 1, \ldots, n_c - 1$; x_1 and $x_{w\,CO_2}$ in terms of the remaining $n_c + 1$ unknowns x_i, $i = 2, \ldots, n_c - 1$; S_w, S_g, and p_o. The remaining $n_c + 1$ unknowns are the primary unknowns, while the eliminated unknowns are secondary unknowns used in this work (Table 2). The linearized primary equations, after eliminating the secondary unknowns using the constraint equations, form a set of $n_c + 1$ equations in terms of $n_c + 1$ primary unknowns, and the linear system

Table 1 Equations and unknown variables in the reservoir simulation model

	Type	Number
Equations	F_i	n_c
	F_w	1
	F_{eh}, F_{ew}	n_c+1
	F_{pcow}, F_{pcgo}	2
	F_s	1
	F_{po}, F_{pg}, F_{pw}	3
	Total	$2n_c+8$
Variables	p_p	3
	S_p	3
	x_i	n_c
	y_i	n_c
	$x_{w\,CO_2}$, $x_{w\,H_2O}$	2
	Total	$2n_c+8$

Table 2 Primary and secondary variables in the case of the three-phase block

Type	Equation	Variable
Primary	F_i	$p_o, S_o, x_i \ \ (i = 1, \ldots, n_c - 1)$
	F_w	S_g
Secondary	F_{eh}	$x_i, y_i \ \ (i = 1, \ldots, n_c - 1)$
	F_{ew}	$x_{w\,CO_2}$

Table 3 Primary variable selection

Type	Variable	F_{ew}
Water–oil–gas	$p_o, S_o, S_g, x_i \ \ (i = 2, \ldots, n_c - 1)$	$F_{ew} = f_{CO_2,w} - f_{CO_2,o} = 0$
Water–oil	$p_o, S_o, x_i \ \ (i = 1, \ldots, n_c - 1)$	$F_{ew} = f_{CO_2,w} - f_{CO_2,o} = 0$
Water–gas	$p_o, S_o, y_i \ \ (i = 1, \ldots, n_c - 1)$	$F_{ew} = f_{CO_2,w} - f_{CO_2,g} = 0$

is solved iteratively, and the secondary unknowns are then computed through back-substitution.

To initialize the simulation, a two-phase oil–gas flash is performed first to compute oil and gas compositions and densities (for the three-phase block), and CO_2 mol fraction in water is assigned to zero for all grid blocks. Aqueous phase properties are calculated from empirical correlations. During simulation, a flash calculation is performed in Newton iterations with mass balance equations. Table 3 lists the selection of primary variables when phase appearance or disappearance happens.

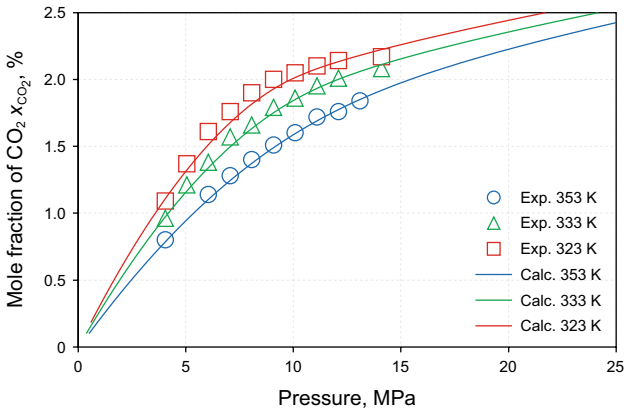

Fig. 1 Pressure–mole fraction diagram of CO_2 at 323, 333, and 353 K calculated from the PR EOS with the WS mixing rule. Experimental data are taken from Bamberger et al. (2000)

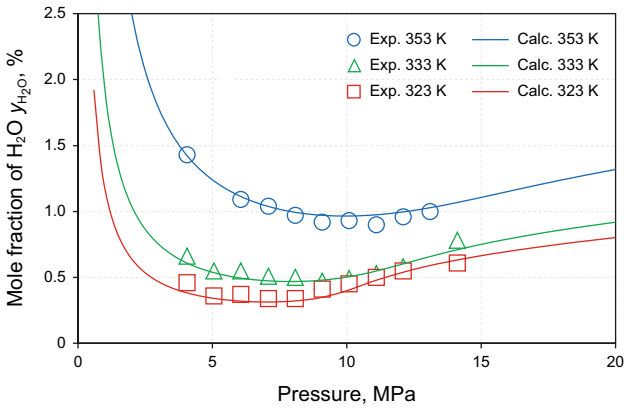

Fig. 2 Pressure–mole fraction diagram of H_2O at 323, 333, and 353 K calculated from the PR EOS with the WS mixing rule. Experimental data are taken from Bamberger et al. (2000)

3.2 Fugacity of CO_2 in water

PR EOS with the WS mixing rule with the NRTL model is used to calculate CO_2 fugacity and its derivative in water. "Appendix 1" gives the derivation of the WS mixing rule for PR EOS (Wong and Sandler 1992). The calculation procedure is: (1) A successive substitution method is used to apply a flash calculation for the binary CO_2/water system, (2) interaction parameters for the WS mixing rule at the specified reservoir temperature are evaluated by fitting experimental data using flashing results, and (3) fitting parameters and PR EOS with the WS mixing rule are used to generate CO_2 fugacity and derivatives in reservoir simulation.

Experimental data used in this work are from Bamberger et al. (2000) for the high-pressure (vapor–liquid) equilibrium of binary systems of CO_2/water from 313 to 353 K and pressures between 1 and 14 MPa. Figures 1

Table 4 Interaction parameters of the WS mixing rule evaluated from fitting published literature data (Bamberger et al. 2000) for the binary CO_2–H_2O system

T, K	τ_{ij}	τ_{ji}	α	k_{ij}	k_{ji}
323	4.3870	0.3930	0.1141	0.3073	0.3073
333	4.3570	0.4130	0.1120	0.3073	0.3073
353	4.1270	0.4530	0.1041	0.3073	0.3073

and 2 show comparisons of the measured data and the calculated results, and Table 8 (Appendix 2) displays the calculated results. The absolute deviation of the calculated composition from the experimental data for CO_2 is around 2%. Table 4 lists the evaluated interaction parameters at temperatures of 323, 333, and 353 K. The interaction data at 333 K are used in the following simulation examples of CO_2 flooding.

The calculated fugacity in distilled water can be adjusted further for the effect of salinity to obtain the fugacity of CO_2 in brine:

$$\ln\left(\frac{f_{is}}{f_i}\right) = k_{is} m_s. \tag{14}$$

Clever and Holland (1968) and Bakker (2003) give the salting-out coefficients for the CO_2/NaCl system, both of which achieve satisfactory results. Bakker's k_{is} is given by:

$$k_{CO_2,s} = 0.11572 - 6.0293 \times 10^{-4} T_{cels} + 3.5817 \times 10^{-6} T_{cels}^2 - 3.7772 \times 10^{-9} T_{cels}^3. \tag{15}$$

Figure 3 displays a pressure–mole fraction diagram of CO_2 at 323, 333, and 353 K calculated from the PR EOS with the WS mixing rule at a salinity of 4 and 6 mol/kg. It achieves a good match with the experimental data from Rumpf et al. (1994), which indicates that the proposed fugacity-adjust method is reliable.

3.3 Aqueous phase properties

Aqueous phase properties, like formation volume factor (B_w), water compressibility (c_w), and water viscosity, can be simply correlated with the methods displayed in "Appendix 3." Initially, B_w and c_w should be evaluated at the CO_2 saturated condition. For an undersaturated condition, linear interpolation is suggested by Chang et al. (1998). However, we found that aqueous phase properties are virtually proportional to the CO_2 solubility. Hence, we replaced R_{sw} in Eqs. 35 and 37 with the mole fraction of CO_2 in water to avoid cumbersome CO_2 solubility prediction. This assumption introduces trivial error for the undersaturated condition because no more than a few percent of CO_2 is in the aqueous phase. The effect of gas on aqueous viscosity is not considered because it was found to be very small (Whitson and Brulé 2000).

4 Simulation results

The simulation described here includes one- and three-dimensional CO_2 flooding problems. For each problem, the PR–WS model is compared to the conventional model where the solubility of CO_2 in water is ignored. Water is present but is immobile in all calculations to have a better understanding of phase equilibria of CO_2. The CO_2/methane/butane/decane system is used for the hydrocarbon content. The reservoir temperature is 333 K for all calculations, and interaction parameters for the WS mixing rule are taken from the evaluated data in Table 4 at 333 K. The capillary force, dispersion, and gravity are neglected for all simulations.

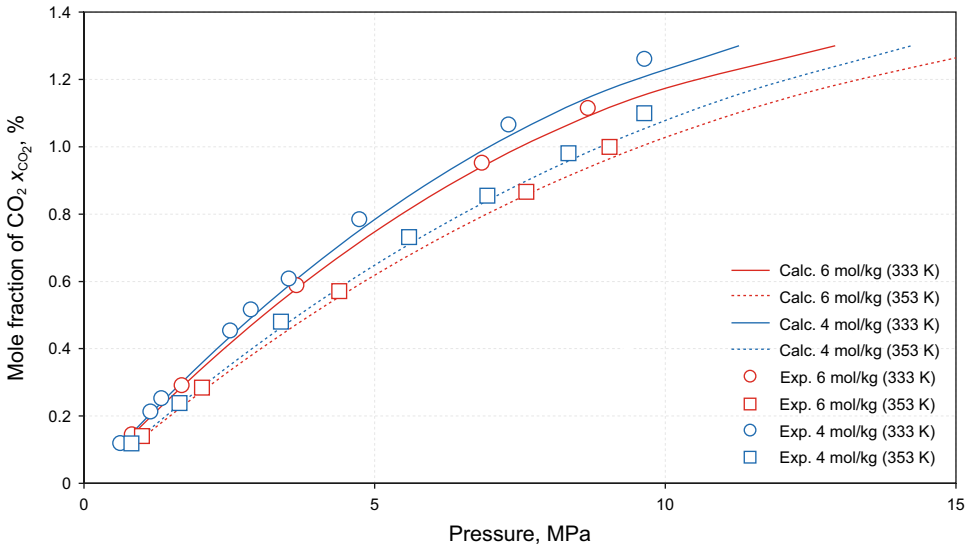

Fig. 3 Pressure–mole fraction diagram of CO_2 at 323 and 353 K calculated by the PR EOS with WS mixing rule at a salinity of 4 and 6 mol/kg. Experimental data are taken from Rumpf et al. (1994)

4.1 One-dimensional CO_2 flooding

Four runs are designed to simulate a one-dimensional CO_2 flooding problem. The model uses a number of $20\times1\times1$ grid blocks with dimensions of 7.5 m × 60 m × 30 m. Permeability and porosity are 20 mD and 0.2, respectively. To investigate the adverse effects of CO_2 solubility on the oil recovery, the following simplifications are included: (1) Water compressibility and rock compressibility are zero and (2) water viscosity is a constant with a value of 0.5 cP. The initial oil composition is 0.05/0.15/0.2/0.6 for the CO_2/methane/butane/decane system. The initial water saturation of run1, run2, and run3 is 0.2, 0.4, and 0.6, respectively. No gas is present at the beginning of the simulation. An injection well injects CO_2 at $x=150$ with a gas rate of 4500 m^3/d at standard conditions, and a production well produces at $x=0$ on deliverability at 14 MPa (Table 5).

Figure 4 shows oil and gas rates at the standard condition versus time, and Fig. 5 displays the oil recovery factor versus time simulated by the PR–WS model and the conventional model. For convenience, an asterisk (*) is appended to the name of simulation results of the conventional model. ΔRF_{max} is defined as the maximum absolute difference of recovery factors calculated by the PR–WS and conventional models within the time span. The turning point is defined as the limit where the oil rate of the PR–WS model starts to exceed that of the conventional model, which indicates that delayed oil is going to be recovered.

The oil and gas rate in run1 calculated by the PR–WS model is slightly lower than the conventional model because there is not much water present in the reservoir ($S_w=0.2$). Run1 does not reach its turning point on account of too short production time or too small CO_2 injection rate. ΔRF_{max} is at the end of the simulation with a value of 0.73%. Run2 displays a significant difference between the oil and gas rates of the PR–WS and conventional models. The turning point is around 1550 days. ΔRF_{max} locates at the turning point with a value of 1.93%, which shows around 2% of oil recovery is delayed. The phenomenon of delaying is enlarged in run3 when water saturation is increased to 0.6. This simulation shows that 4.11% of recovery is delayed, and the turning point is advanced to 1050 days. We observe that for a constant CO_2 injection rate, the amount of oil present in the reservoir is a key factor which influences the time of the turning point, while the amount of water is a key factor which affects the value of ΔRF_{max}. Finally, the gas rate of the PR–WS model in the three runs is always smaller than the conventional model because a significant portion of injected CO_2 is dissolved in water, which can be considered as "lost" in the aqueous phase.

To further understand the CO_2 equilibria between water and oil, Fig. 6 shows CO_2 and decane distribution versus distance for the PR–WS model and conventional models, and

Table 5 Model data of the one-dimensional problem

Item	Value
Reservoir length, m	150
Reservoir width, m	60
Reservoir thickness, m	30
Permeability, mD	20
Porosity	0.2
Grid blocks in the x, y, z directions	$20\times1\times1$
Capillary pressure	0
Water compressibility c_w, MPa^{-1}	0
Compressibility, MPa^{-1}	0
Relative permeability data	
S_{wc}	0.2
S_{org}	0.2
S_{gc}	0
S_{gr}	0.15
K_{rocw}	1.0
K_{rgcw}	1.0
K_{rw}	0
Water viscosity, cP	0.5 (constant)
Initial pressure, MPa	14
Reservoir temperature, K	333
Initial oil composition (CO_2, C_1, C_4, C_{10}), mol%	0.05, 0.15, 0.2, 0.6
Initial saturation (S_w, S_o, S_g)	
run1	0.2, 0.8, 0.0
run2	0.4, 0.6, 0.0
run3	0.6, 0.4, 0.0
The standard conditions	
Pressure, MPa	0.101325
Temperature, K	288.71
WS mixing rule parameters	From Table 4 at 333 K

Fig. 7 displays the mole fraction of CO_2 in brine versus distance at the time 600, 1200, and 1800 days for the three runs. With the advance of CO_2 into the reservoir, mole fractions of hydrocarbon components like decane gradually decrease along the displacing direction. The solubility of CO_2 in the one-dimensional problem at 14 MPa with a 4 mol/kg of sodium chloride is 1.4% (mol/mol) (0.80 mol/kg). These distribution curves show that CO_2 breakthrough happens before the turning point because only half of the reservoir water is in a saturated condition at the breakthrough (as shown in run2 at 1200 days).

Figure 8 shows the ratio of injected CO_2 dissolved in the aqueous phase. From run1 to run3, 2%, 4%, and 7% of injected CO_2 is dissolved in the aqueous phase, respectively. The amount of CO_2 that dissolved in the aqueous phase, in the three runs, is nearly proportional to the water saturation in the reservoir, which indicates that if water alternating gas is implemented or CO_2 is injected after water flooding, the

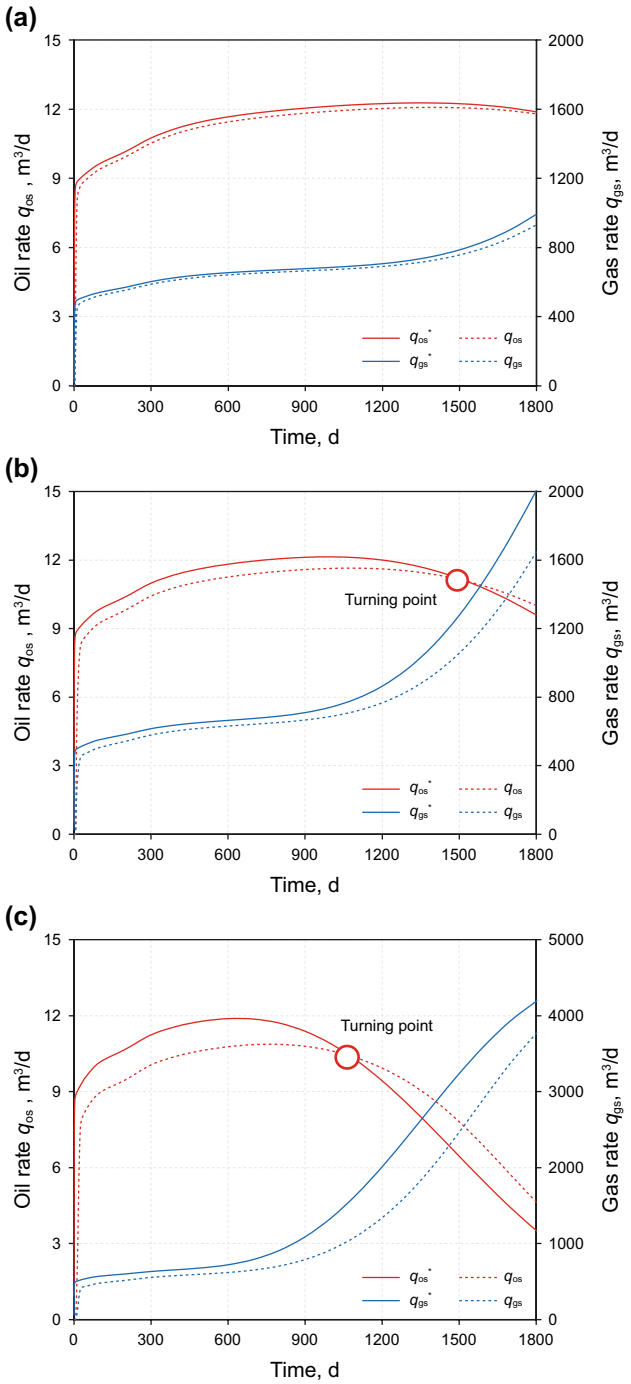

Fig. 4 Oil and gas rates at standard conditions versus time simulated by the PR–WS model (dashed line) and the conventional model (solid line with an asterisk (*) appended to the name of the legend). **a** run1. **b** run2. **c** run3

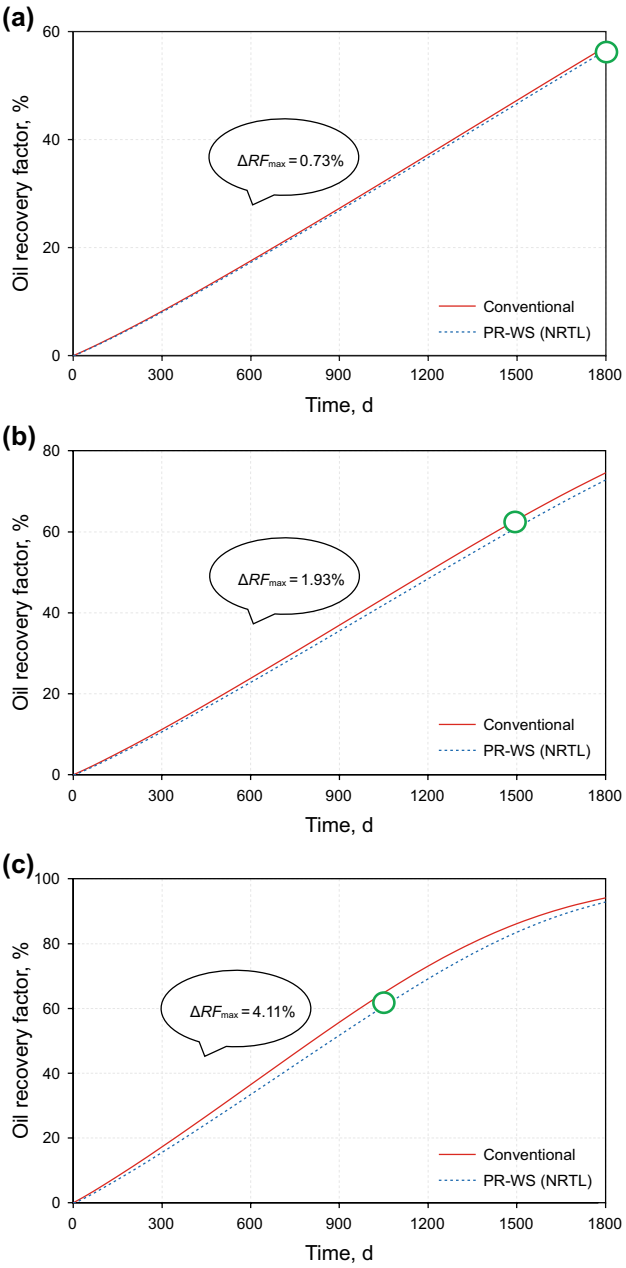

Fig. 5 Oil recovery factor versus time simulated by the conventional model and the PR–WS model (ΔRF_{max} is defined as the maximum absolute difference of recovery factors calculated by the two models within the simulation span). **a** run1. **b** run2. **c** run3

solubility effects of CO_2 should be highly pronounced. We next investigate the influence of salinity on the dissolution of CO_2 in the aqueous phase. The model setup is the same as run2 except for the salinity: run2_0 means zero salinity, while run2_4 means 4 mol/kg salinity in the aqueous phase.

Figure 9 displays a comparison of CO_2 solubility in water for run2_4 and run2_0 at the time 600, 1200, and 1800 days. Zero salinity increases CO_2 solubility in water from 1.4% to 2.1% (mol/mol). Besides, the ratio of injected CO_2 dissolved in the aqueous phase also increases from 4.0% to 6.4% for run2_4.

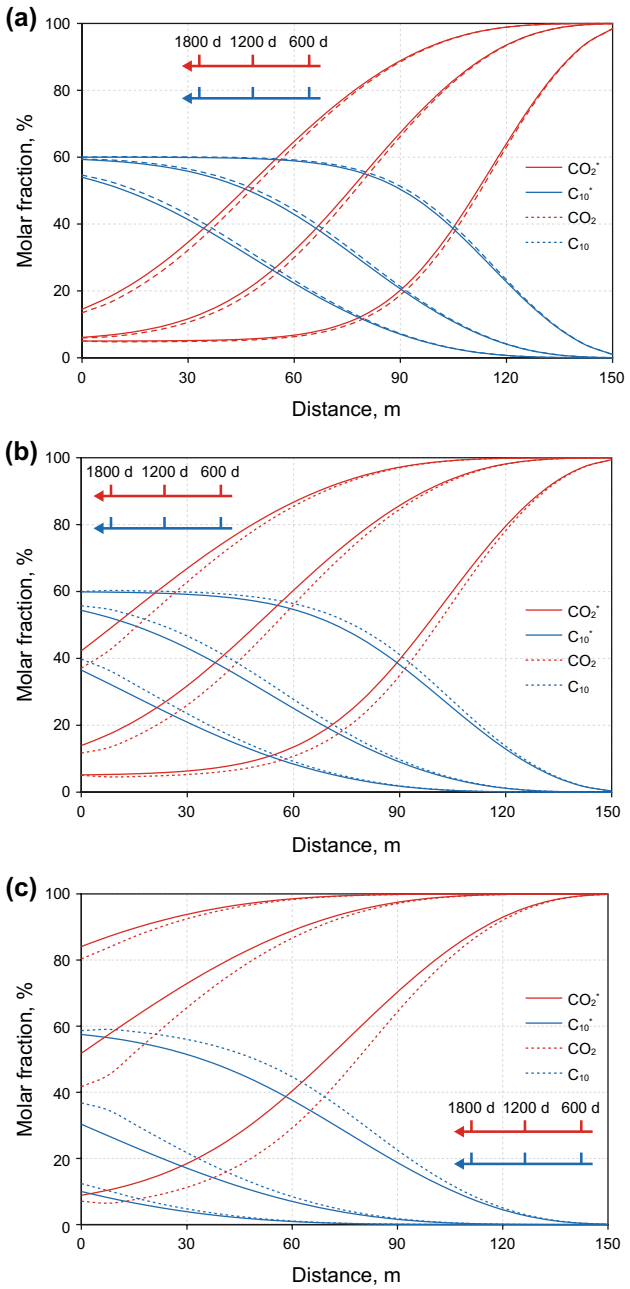

Fig. 6 CO_2 and decane distributions versus distance at the times 600, 1200, and 1800 days (the coordinate axis in the figure indicates the displacement direction and the component distribution at the different time) **a** run1. **b** run2. **c** run3

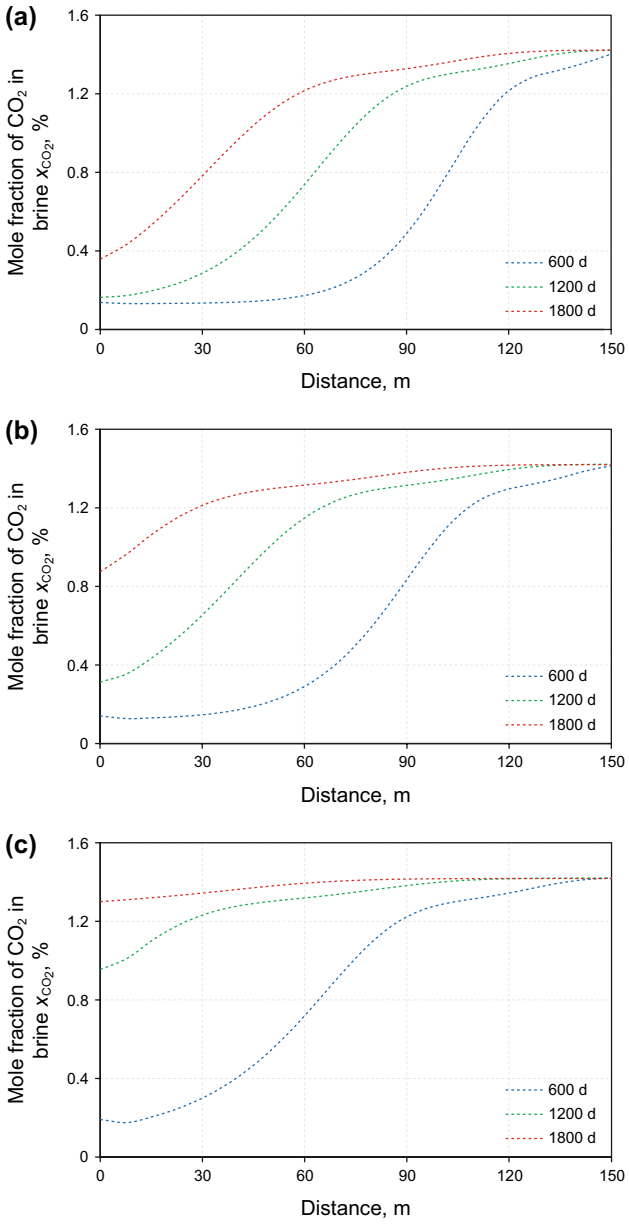

Fig. 7 Mole fraction of CO_2 in brine versus distance at the time 600, 1200, and 1800 days for the three runs. **a** run1. **b** run2. **c** run3

4.2 Three-dimensional CO_2 flooding

The model used to simulate a three-dimensional CO_2 flooding problem is derived from the SPE1 project (Odeh 1981). CO_2 is injected into a stratified reservoir with an anisotropic permeability of 500, 50, and 200 mD in the three layers with a thickness of 20, 30, and 50 ft. The porosity is uniform and equal to 0.3. Relative permeability

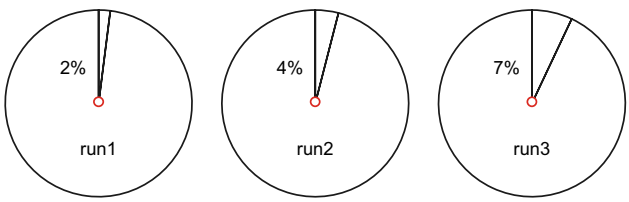

Fig. 8 Ratio of injected CO_2 dissolved in the aqueous phase for the three runs

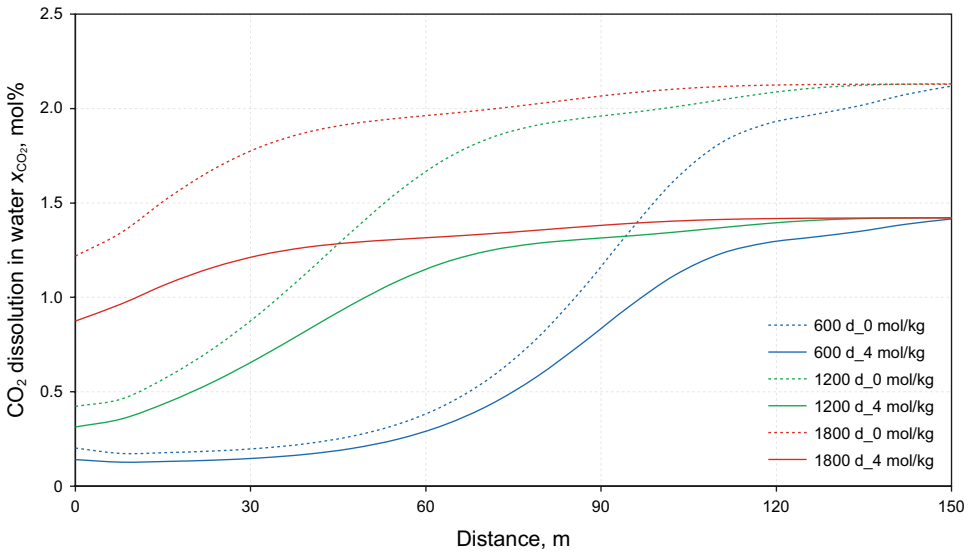

Fig. 9 Comparison of the CO_2 dissolution in water at zero and 4 mol/kg of NaCl in run2 at the time 600, 1200, and 1800 days

data, initial oil composition, reservoir temperature, and injection and production schemes are inherited from the one-dimensional simulation. Aqueous properties, like formation volume factor (B_w), water compressibility (c_w), and water viscosity, are calculated by correlations in "Appendix 3." We denote this simulation as run_SPE1 (Table 6).

Figure 10 displays the mole fraction of CO_2 in brine in the 300 grid blocks at the time 4000, 8000, and

Table 6 Model data of three-dimensional problem

Item	Value
Permeability of three layers k_1, k_2, k_3, mD	500, 50, 200
Porosity	0.3
Grid blocks in the x, y, z directions	$10\times10\times3$
Dimensions (x, y, z), m	$x=305$, $y=305$, $z_1=6.10$, $z_2=9.14$, $z_3=15.24$
Capillary pressure	0
Water compressibility c_w, MPa^{-1}	Correlated with "Appendix 3"
Compressibility, MPa^{-1}	4.35×10^{-4}
Relative permeability data	
S_{wc}	0.2
S_{org}	0.2
S_{gc}	0
S_{gr}	0.15
K_{rocw}	1.0
K_{rgcw}	1.0
K_{rw}	0
Water viscosity, cP	Correlated with "Appendix 3"
Water formation volume factor	Correlated with "Appendix 3"
Initial pressure, MPa	14
Reservoir temperature, K	333
Initial oil composition (CO_2, C_1, C_4, C_{10}), mol%	0.05, 0.15, 0.2, 0.6
Initial saturation (S_w, S_o, S_g)	0.4, 0.6, 0.0
The standard conditions	
Pressure, MPa	0.101325
Temperature, K	288.71
WS mixing rule parameters	From Table 4 at 333 K

14,600 days, respectively. The injected CO_2 travels much faster in the upper layer ($k_1 = 500$ mD) as its permeability is higher than the other two layers. A gas breakthrough is going to happen because the injected CO_2 spreads to the production well (the grid painted in warm color in Fig. 10c). A sharp increase in the gas rate in Fig. 11 also affirms the gas breakthrough. In addition, the oil rates from the PR–WS model and the conventional model are very close at the end of the simulation, indicating a turning point in the near future. Finally, it is easy to draw a conclusion that around 1% of oil recovery is delayed and 5% of injected CO_2 is dissolved in the aqueous phase (Fig. 12).

Highly stratified reservoirs cause uneven displacement in this simulation. Although CO_2 is injected in the lower layer ($k_3 = 200$ mD), it travels much faster in the upper layer (k_1)

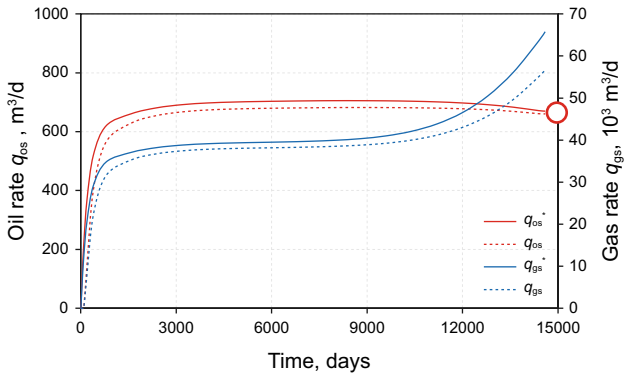

Fig. 11 Oil and gas rates at the standard conditions versus time simulated by the conventional and PR–WS models

Fig. 10 Mole fraction of CO_2 in brine in 300 grid blocks at time 4000 days (**a**), 8000 days (**b**), and 14600 days (**c**)

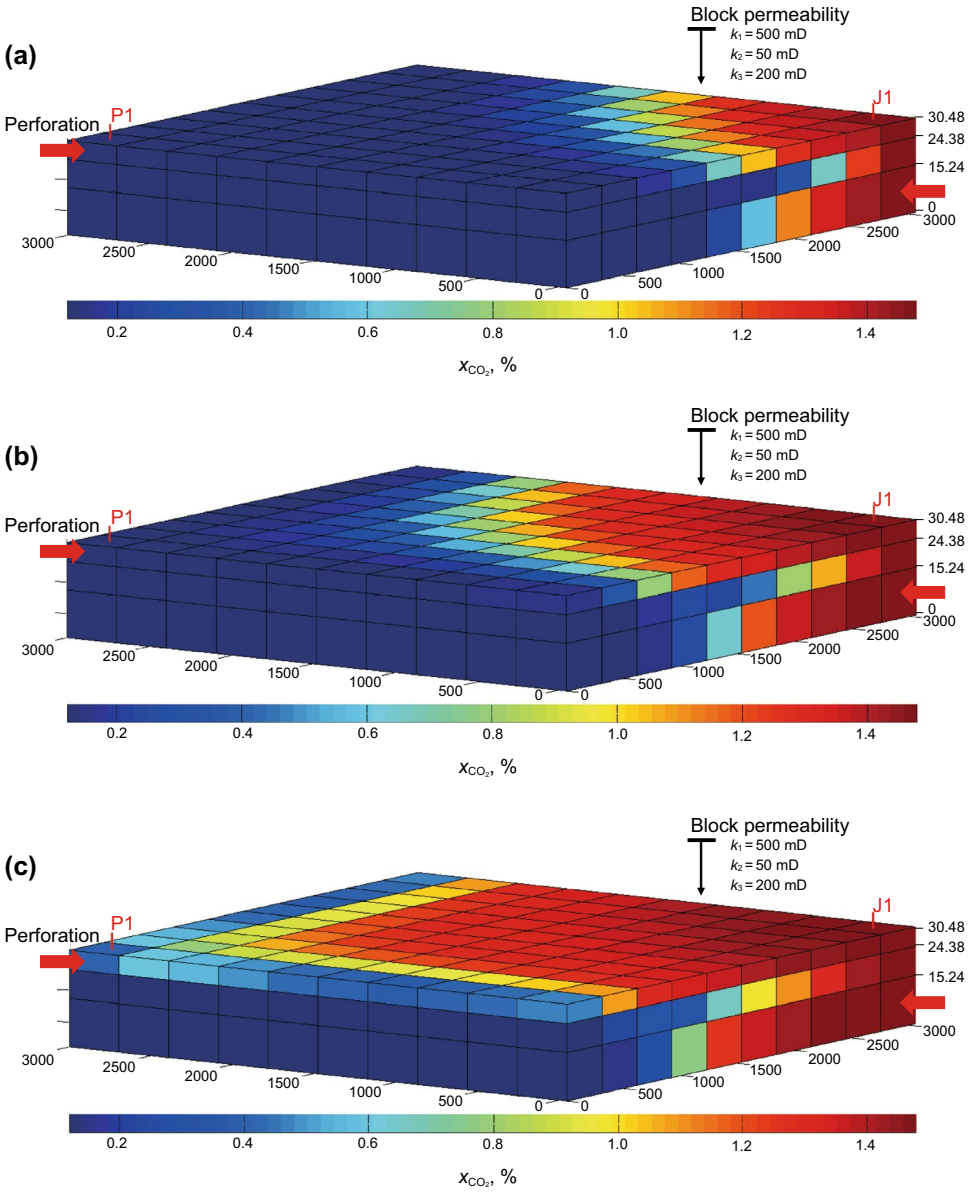

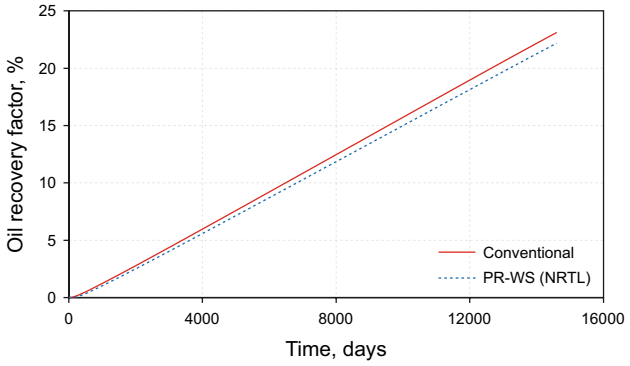

Fig. 12 Oil recovery factor versus time simulated by the conventional and PR–WS models

compared to the other two layers. We can speculate that a serious gas breakthrough will happen in the upper layer (k_1). In this case, mobility control measures like water alternating gas or simultaneous water alternating gas will be helpful, and certainly, the adverse effect of CO_2 solubility in water should be more pronounced than in this example. Moreover, neglecting gravity may fail to consider the upward migration of CO_2 due to the buoyancy, thereby mispredicting the development of CO_2 flooding. For example, if CO_2 is injected at the bottom of the oil-bearing layer where the permeability is relatively high, neglecting the gravity would underestimate the oil recovery because the simulation wrongly predicts a quick gas breakthrough in the bottom layer. On the contrary, such as the run_SPE1, neglecting the gravity would overestimate the performance because the simulation delays the gas breakthrough in the upper layer. For a high permeable reservoir, the gravity effect is trivial because CO_2 moves much faster horizontally than vertically, but for a unconventional formation, considering the effect of gravity is recommended to achieve an accurate simulation result.

4.3 The efficiency of the formulation

Computing time required for a formulation is of interest since a comparison of overall efficiencies of different formulations is helpful in continuing development efforts. Table 7 lists the average number of iterations needed per time step for the PR–WS and conventional models and their time ratio in the five runs. Figure 13 shows these results in a graph for comparison. For CO_2 injection problems, the conventional model converges in 3–7 Newton iterations per time step with an average value of 4.51, and the PR–WS model needs 4–8 iterations with an average value of 5.34. Generally, the PR–WS model spends 57% more time than the conventional model. Calculating CO_2 fugacity and its derivatives in the aqueous phase is time-consuming, which is the main reason why the computational complexity is significantly increased.

Table 7 Newton iteration per time step and time ratio in the five runs (time ratio is defined as the ratio of simulation time of the PR–WS model and the conventional model)

	Time ratio	Conventional model	PR–WS model
run1	1.54	3.86	4.61
run2	1.55	4.07	5.00
run3	1.59	4.46	5.46
run_s	1.60	4.07	5.00
run_SPE1	1.57	6.07	6.61
Average	1.57	4.51	5.34

5 Conclusions

An implicit formulation has been described for simulation of three-dimensional CO_2 flooding problems, including CO_2 equilibria between water and oil. In this model, the aqueous phase is treated as a binary CO_2/water system and only CO_2 is considered mutually soluble in the aqueous phase and the hydrocarbon phase. The fugacity of CO_2 in the aqueous phase is calculated by PR EOS and WS mixing rule with NRTL parameters, while oil- and gas-phase densities and fugacities are modeled by PR EOS with a one-fluid mixing rule. Detailed findings are summarized as follows:

1. PR EOS and the WS mixing rule with the NRTL model are an accurate approach to predict the phase behavior of the binary CO_2/water system. The proposed method with salinity effect correction achieves a good match with the experimental data.
2. Selecting natural variables and full implicit natural variables of the PR–WS model enhances efficiency as well as reliability. For the test example of CO_2 flooding, this model converges in 4–8 iterations per time step and the total simulation time is 57% more than the conventional model.
3. CO_2 flooding examples show that a significant amount of injected CO_2 is dissolved in water and is unavailable

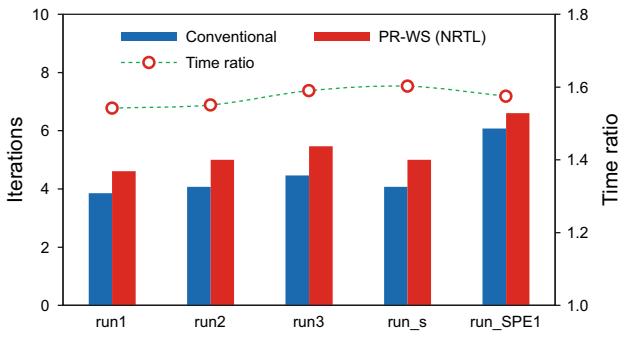

Fig. 13 Comparison of Newton iterations per time step and time ratio in the five runs

for mixing with oil. For example, the run3 displays up to 7% of injected CO_2 is dissolved in the aqueous phase, which results in a delayed oil recovery of 4%.

4. The gas rate of the PR–WS model in all examples is smaller than the conventional model because a significant portion of injected CO_2 is dissolved in water, which can be considered as "lost" in the aqueous phase.
5. CO_2 breakthrough happens in advance of the turning point where the delayed oil starts to be recovered. In field applications, the delayed oil is hard to recover due to serious gas breakthrough.

Acknowledgements This work was financially supported by National Natural Science Foundation of China (U1762101) and National Science and Technology Major Projects (2017ZX05069). Special thanks for Changqing Oilfield for providing detailed geology and production data. We would like to express our heartfelt gratitude to Professor Haining Zhao for his constructive suggestion about this paper. Computer Modeling Group are also acknowledged for offering CMG software.

Appendix 1

Peng and Robinson (1976) proposed the following modification of the van der Waals equation of state:

$$P = \frac{RT}{\left(\underline{V} - b\right)} - \frac{a(T)}{\underline{V}^2 + 2b\underline{V} - b^2}. \tag{16}$$

The Helmholtz free energy departure function for the Peng–Robinson equation at a given temperature, pressure, and composition is:

$$\frac{\underline{A} - \underline{A}^{\mathrm{IGM}}}{RT} = -\ln\left[\frac{P\left(\underline{V} - b\right)}{RT}\right] + \frac{a}{2\sqrt{2}bRT}\ln\left[\frac{\underline{V} + \left(1 - \sqrt{2}\right)b}{\underline{V} + \left(1 + \sqrt{2}\right)b}\right]. \tag{17}$$

In the limit of pressure going to infinity, this becomes:

$$\lim_{P\to\infty}\frac{\left(\underline{A} - \underline{A}^{IG}\right)}{RT} = \frac{a}{bRT}C, \tag{18}$$

with the constant C being:

$$C = \frac{1}{\sqrt{2}}\ln\left(\sqrt{2} - 1\right). \tag{19}$$

Therefore, the excess Helmholtz free energy at infinite pressure $\underline{A}^E_\infty/(RT)$ is:

$$\frac{\underline{A}^E_\infty}{CRT} = \frac{a_{\mathrm{m}}}{b_{\mathrm{m}}RT} - \sum_i x_i\frac{a_i}{b_iRT}. \tag{20}$$

PR EOS parameters a_{m} and b_{m} can be obtained as follows.

$$b_{\mathrm{m}} = \frac{Q}{1 - D} \tag{21}$$

and

$$\frac{a_{\mathrm{m}}}{RT} = Q\frac{D}{1 - D}, \tag{22}$$

with Q and D defined as:

$$Q = \sum_i\sum_j x_ix_j\left(b - \frac{a}{RT}\right)_{ij}, \tag{23}$$

and

$$D = \sum_i x_i\frac{a_i}{b_iRT} + \frac{\underline{A}^E_\infty}{CRT}. \tag{24}$$

The thermodynamic properties of a mixture can now be calculated. The fugacity coefficient is computed from:

$$\ln\varphi_i = \int_{\underline{V}}^{\infty}\left[\frac{1}{RT}\left(\frac{\partial P}{\partial n_i}\right)_{T,V,n_j} - \frac{1}{\underline{V}}\right]\mathrm{d}\underline{V} - \ln\left(\frac{P\underline{V}}{RT}\right). \tag{25}$$

For the Peng–Robinson equation of state and an arbitrary set of mixing rules for a_m and $b_{m,}$

$$\ln\varphi_i = -\ln\left[\frac{P\left(\underline{V} - b_{\mathrm{m}}\right)}{RT}\right] + \frac{1}{b_{\mathrm{m}}}\left(\frac{\partial nb_{\mathrm{m}}}{\partial n_i}\right)\left(\frac{P\underline{V}}{RT} - 1\right) + \frac{1}{2\sqrt{2}}\left(\frac{a_{\mathrm{m}}}{b_{\mathrm{m}}RT}\right)\left[\frac{1}{a_{\mathrm{m}}}\left(\frac{1}{n}\frac{\partial n^2a_{\mathrm{m}}}{\partial n_i}\right) - \frac{1}{b_{\mathrm{m}}}\left(\frac{\partial nb_{\mathrm{m}}}{\partial n_i}\right)\right]\ln\left[\frac{\underline{V} + b_{\mathrm{m}}\left(1 - \sqrt{2}\right)}{\underline{V} + b_{\mathrm{m}}\left(1 + \sqrt{2}\right)}\right]. \tag{26}$$

The partial derivatives of a_m and b_m are:

$$\frac{\partial nb_m}{\partial n_i} = \frac{1}{1-D}\left(\frac{1}{n}\frac{\partial n^2 Q}{\partial n_i}\right) - \frac{Q}{(1-D)^2}\left(1 - \frac{\partial nD}{\partial n_i}\right) \quad (27)$$

and

$$\frac{1}{RT}\left(\frac{1}{n}\frac{\partial n^2 a_m}{\partial n_i}\right) = D\frac{\partial nb_m}{\partial n_i} + b_m\frac{\partial nD}{\partial n_i}, \quad (28)$$

with the partial derivatives of Q and D given by:

$$\frac{1}{n}\frac{\partial n^2 Q}{\partial n_i} = 2\sum_j x_j\left(b - \frac{a}{RT}\right)_{ij}, \quad (29)$$

and

$$\frac{\partial nD}{\partial n_i} = \frac{a_i}{b_i RT} + \frac{\ln\gamma_{\infty i}}{C}, \quad (30)$$

with

$$\ln\gamma_{\infty i} = \frac{1}{RT}\frac{\partial nA^E_{-\infty}}{\partial n_i}. \quad (31)$$

$A^E_{-\infty}/(RT)$ is calculated by the NRTL model (Renon and Prausnitz 1968):

$$\frac{A^E_{-\infty}}{RT} = \sum_i x_i\left(\frac{\sum_j x_j\tau_{ji}g_{ji}}{\sum_k x_k g_{ki}}\right), \quad (32)$$

with

$$g_{ij} = \exp\left(-\alpha_{ij}\tau_{ij}\right) \quad \left(\alpha_{ij} = \alpha_{ji}\right). \quad (33)$$

In this case, the partial derivatives of $A^E_{-\infty}/(RT)$ with respect to the mole number of each species, which is the logarithm of the species activity coefficient, are given by:

$$\ln\gamma_{\infty i} = \frac{\sum_j x_j\tau_{ji}g_{ji}}{\sum_k x_k g_{ki}} + \sum_j \frac{x_j g_{ij}}{\sum_k x_k g_{kj}}\left(\tau_{ij} - \frac{\sum_l x_l\tau_{lj}g_{lj}}{\sum_k x_k g_{kj}}\right). \quad (34)$$

Appendix 2

See Table 8.

Table 8 Experimental data from Bamberger et al. (2000) and CO_2 and H_2O compositions of the binary CO_2/water system calculated from the PR EOS with the WS mixing rule at 323, 333, and 353 K

T, K	P, MPa	Experimental data for the vapor–liquid equilibrium of the binary CO_2/water system		Calculated CO_2 and H_2O compositions in the binary CO_2/water system		Absolute deviation (AD) of the calculated compositions from the experimental data, %	
		$10^2 x^{exp}_{CO_2}$	$10^2 y^{exp}_{H_2O}$	$10^2 x^{calc}_{CO_2}$	$10^2 y^{calc}_{H_2O}$	CO_2	H_2O
323	4.05	1.09	0.46	1.11	0.38	1.69	16.93
	5.06	1.37	0.36	1.32	0.34	3.32	5.50
	6.06	1.61	0.37	1.51	0.32	6.00	13.71
	7.08	1.76	0.34	1.68	0.31	4.54	7.95
	8.08	1.90	0.34	1.82	0.32	4.33	5.55
	9.09	2.00	0.41	1.93	0.35	3.50	14.92
	10.09	2.05	0.45	2.02	0.41	1.69	10.00
	11.10	2.10	0.50	2.08	0.48	0.92	4.40
	12.10	2.14	0.55	2.13	0.54	0.29	1.83
	14.11	2.17	0.61	2.22	0.63	2.51	3.59
Average AD, %						2.88	8.44
333	4.05	0.96	0.66	0.97	0.61	1.29	7.65
	5.06	1.21	0.55	1.17	0.54	3.51	2.52
	6.06	1.38	0.55	1.34	0.50	2.79	9.97
	7.08	1.57	0.51	1.50	0.47	4.51	7.02
	8.08	1.66	0.50	1.63	0.47	1.53	6.08
	9.09	1.79	0.47	1.75	0.48	2.09	2.09
	10.09	1.86	0.49	1.85	0.51	0.47	3.25
	11.10	1.95	0.53	1.93	0.55	0.82	3.58
	12.10	2.01	0.58	2.00	0.60	0.38	3.99
	14.11	2.08	0.78	2.11	0.71	1.58	8.92

Table 8 continued

T, K	P, MPa	Experimental data for the vapor–liquid equilibrium of the binary CO_2/water system		Calculated CO_2 and H_2O compositions in the binary CO_2/water system		Absolute deviation (AD) of the calculated compositions from the experimental data, %	
		$10^2 x^{exp}_{CO_2}$	$10^2 y^{exp}_{H_2O}$	$10^2 x^{calc}_{CO_2}$	$10^2 y^{calc}_{H_2O}$	CO_2	H_2O
Average AD, %						1.90	5.51
353	4.05	0.80	1.43	0.79	1.42	1.61	0.54
	6.06	1.14	1.09	1.11	1.11	3.04	2.05
	7.08	1.28	1.04	1.25	1.04	2.53	0.25
	8.08	1.40	0.97	1.38	0.99	1.79	2.40
	9.09	1.51	0.92	1.49	0.97	1.20	5.49
	10.09	1.60	0.93	1.60	0.97	0.22	3.78
	11.10	1.72	0.90	1.69	0.97	1.67	8.29
	12.10	1.76	0.96	1.78	1.00	0.89	3.79
	13.10	1.84	1.00	1.85	1.03	0.62	2.82
Average AD, %						1.51	3.27

Appendix 3

Formation volume factor (B_w) and water compressibility (c_w) at the saturated conditions are given by (Whitson and Brulé 2000):

(1) B_w at the saturated conditions:

$$B_w(p_{si}, T_F, R_{sw}) = B^*_w(p_{si}, T_F)\left(1 + 0.0001R^{1.5}_{sw}\right). \quad (35)$$

with

$$B^*_w(p_{si}, T_F) = B^0_w(p_{sc,si}, T_F)\left(1 + \frac{A_1}{A_0}p_{si}\right)^{(1/A_1)}. \quad (36)$$

(2) c_w at the saturated conditions:

$$c_w(p_{si}, T_F, R_{sw}) = c^*_w(p_{si}, T_F)\left(1+0.00877R_{sw}\right). \quad (37)$$

with

$$c^*_w(p_{si}, T_F) = \left(A_0 + A_1 p_{si}\right)^{-1}. \quad (38)$$

where A_0 and A_1 in Eqs. (36) and (38) are calculated by:

$$A_0 = 10^6\left[0.314 + 0.58w_s + \left(1.9\times10^{-4}\right)T_F - \left(1.45\times10^{-6}\right)T^2_F\right]. \quad (39)$$

and

$$A_1 = 8 + 50w_s - 0.125w_sT_F. \quad (40)$$

where c_w is in psi^{-1}, p_{si} in psia, T_F in °F, and w_s in weight fraction of NaCl.

Water viscosity in brine can be calculated from Kestin et al. (1978)

$$\mu_w = \left(1+A_0p\right)\mu^*_w. \quad (41)$$

$$\log\frac{\mu^*_w}{\mu^0_w} = A_1 + A_2\log\frac{\mu^0_w}{\mu^0_{w20}}. \quad (42)$$

$$A_0 = 10^{-3}\left[0.8+0.01\left(T_{cels} - 90\right)\exp\left(-0.25c_{sw}\right)\right]. \quad (43)$$

$$A_1 = \sum_{i=1}^{3} a_{1i}\left(c_{sw}\right)^i. \quad (44)$$

$$A_2 = \sum_{i=1}^{3} a_{2i}\left(c_{sw}\right)^i. \quad (45)$$

$$\log\frac{\mu^0_w}{\mu^0_{w20}} = \sum_{i=1}^{4} a_{3i}\frac{\left(20 - T_{cels}\right)^i}{96 + T_{cels}}. \quad (46)$$

$$\mu^0_{w20} = 1.002\ \text{cP}. \quad (47)$$

where the values of parameter a are listed in Table 9, with μ in cP, T_{cels} in °C, and p in MPa.

Table 9 Values of parameter a in Eqs. 44, 45, and 46

$a_{11} = 3.324\times10^{-2}$	$a_{21} = -3.96\times10^{-2}$	$a_{31} = 1.2378$
$a_{12} = 3.624\times10^{-3}$	$a_{22} = 1.02\times10^{-2}$	$a_{32} = -1.303\times10^{-3}$
$a_{13} = -1.879\times10^{-4}$	$a_{23} = -7.02\times10^{-4}$	$a_{33} = 3.060\times10^{-6}$
		$a_{34} = 2.550\times10^{-8}$

References

Bakker RJ. Package FLUIDS 1. Computer programs for analysis of fluid inclusion data and for modelling bulk fluid properties. Chem Geol. 2003;194(1–3):3–23. https://doi.org/10.1016/S0009-2541(02)00268-1.

Bamberger A, Sieder G, Maurer G. High-pressure (vapor + liquid) equilibrium in binary mixtures of (carbon dioxide + water or acetic acid) at temperatures from 313 to 353 K. J Supercrit Fluids. 2000;17(2):97–110. https://doi.org/10.1016/S0896-8446(99)00054-6.

Chang YB, Coats BK, Nolen JS. A compositional model for CO_2 floods including CO_2 solubility in water. SPE Reserv Eval Eng. 1998;1(02):155–60. https://doi.org/10.2118/35164-PA.

Chien MCH, Lee ST, Chen WH. A new fully implicit compositional simulator. In: SPE reservoir simulation symposium, Dallas, Texas, 10–13 February 1985. https://doi.org/10.2118/13385-MS.

Cho J, Kim TH, Lee KS. Compositional modeling and simulation of dimethyl ether (DME)-enhanced waterflood to investigate oil mobility improvement. Pet Sci. 2018;15(2):297–304. https://doi.org/10.1007/s12182-017-0212-z.

Clever HL, Holland CJ. Solubility of argon gas in aqueous alkali halide solutions. J Chem Eng Data. 1968;13(3):411–4. https://doi.org/10.1021/je60038a033.

Coats KH. An equation of state compositional model. SPE J. 1980;20(05):363–76. https://doi.org/10.2118/8284-PA.

Enick RM, Klara SM. CO_2 solubility in water and brine under reservoir conditions. Chem Eng Commun. 1990;90(1):23–33. https://doi.org/10.1080/00986449008940574.

Enick RM, Klara SM. Effects of CO_2 solubility in brine on the compositional simulation of CO_2 floods. SPE Reserv Eng. 1992;7(02):253–8. https://doi.org/10.2118/20278-PA.

Fussell LT, Fussell DD. An iterative technique for compositional reservoir models. SPE J. 1979;19(04):211–20. https://doi.org/10.2118/6891-PA.

Guo H, Chen Y, Hu Q, et al. Quantitative Raman spectroscopic investigation of geo-fluids high-pressure phase equilibria: part I. accurate calibration and determination of CO_2 solubility in water from 273.15 to 573.15 K and from 10 to 120 MPa. Fluid Phase Equilib. 2014;382(1):70–9. https://doi.org/10.1016/j.fluid.2014.08.032.

Huron MJ, Vidal J. New mixing rules in simple equations of state for representing vapour-liquid equilibria of strongly non-ideal mixtures. Fluid Phase Equilib. 1979;3(4):255–71. https://doi.org/10.1016/0378-3812(79)80001-1.

Ju B, Wu Y, Qin J, et al. Modeling CO_2 miscible flooding for enhanced oil recovery. Pet Sci. 2012;9(2):192–8. https://doi.org/10.1007/s12182-012-0199-4.

Jaubert JN, Mutelet F. VLE predictions with the Peng–Robinson equation of state and temperature dependent kij, calculated through a group contribution method. Fluid Phase Equilib. 2004;224(2):285–304. https://doi.org/10.1016/j.fluid.2004.06.059.

Jaubert JN, Privat R, Mutelet F. Predicting the phase equilibria of synthetic petroleum fluids with the PPR78 approach. AIChE J. 2010;56(12):3225–35. https://doi.org/10.1002/aic.12232.

Kestin J, Khalifa HE, Abe Y, et al. Effect of pressure on the viscosity of aqueous sodium chloride solutions in the temperature range 20–150 °C. J Chem Eng Data. 1978;23(4):328–36. https://doi.org/10.1021/je60079a011.

King MB, Mubarak A, Kim JD, et al. The mutual solubilities of water with supercritical and liquid carbon dioxides. J Supercrit Fluids. 1992;5(4):296–302. https://doi.org/10.1016/0896-8446(92)90021-B.

Li YK, Nghiem LX. Phase equilibria of oil, gas and water/brine mixtures from a cubic equation of state and Henry's Law. Can J Chem Eng. 1986;64(3):486–96. https://doi.org/10.1002/cjce.5450640319.

Lohrenz J, Bray BG, Clark CR. Calculating viscosities of reservoir fluids from their compositions. J Pet Technol. 1964;16(10):1171–6. https://doi.org/10.2118/915-PA.

Odeh AS. Comparison of solutions to a three-dimensional black-oil reservoir simulation problem (includes associated paper 9741). J Pet Technol. 1981;33(1):13–25. https://doi.org/10.2118/9723-PA.

Pedersen KS, Milter J, Rasmussen CP. Mutual solubility of water and reservoir fluid at high temperatures and pressures: experimental and simulated data. Fluid Phase Equilib. 2001;189(1–2):85–97. https://doi.org/10.1016/S0378-3812(01)00562-3.

Peng DY, Robinson DB. A new two-constant equation of state. Ind Eng Chem Fundam. 1976;15(1):59–64. https://doi.org/10.1021/i160057a011.

Renon H, Prausnitz JM. Local compositions in thermodynamic excess functions for liquid mixtures. AIChE J. 1968;14(1):135–144. https://doi.org/10.1002/aic.690140124.

Rumpf B, Nicolaisen H, Öcal C, et al. Solubility of carbon dioxide in aqueous solutions of sodium chloride: experimental results and correlation. J. Solut Chem. 1994;23(3):431–48. https://doi.org/10.1007/BF00973113.

Spycher N, Pruess K, Ennis-King J. CO_2–H_2O mixtures in the geological sequestration of CO_2. I. assessment and calculation of mutual solubilities from 12 to 100 °C and up to 600 bar. Geochimica Cosmochimica Acta. 2003;67(16):3015–31. https://doi.org/10.1016/S0016-7037(03)00273-4.

Valderrama JO. The state of the cubic equations of state. Ind Eng Chem Res. 2003;42(8):1603–18. https://doi.org/10.1021/ie020447b.

Valtz A, Chapoy A, Coquelet C, et al. Vapour-liquid equilibria in the carbon dioxide-water system, measurement and modeling from 278.2 to 318.2 K. Fluid Phase Equilib. 2004;226(1):333–44. https://doi.org/10.1016/j.fluid.2004.10.013.

Whitson CH, Brulé MR. Water/hydrocarbon systems. In: Phase behavior, 1st edn. Chap. 9. Richardson: Henry L. Doherty Memorial Fund of AIME, Society of Petroleum Engineers. 2000. p. 142–151.

Wong DSH, Sandler SI. A theoretically correct mixing rule for cubic equations of state. AIChE J. 1992;38(5):671–80. https://doi.org/10.1002/aic.690380505.

Yan W, Stenby EH. The influence of CO_2 solubility in brine on CO_2 flooding simulation. In: SPE annual technical conference and exhibition, New Orleans, Louisiana, 4–7 October, 2009. https://doi.org/10.2118/124628-MS.

Yan W, Stenby EH. The influence of CO_2 solubility in brine on simulation of CO_2 injection into water flooded reservoir and CO_2 WAG. In: SPE EUROPEC/EAGE annual conference and exhibition, Barcelona, Spain, 14–17 June, 2010. https://doi.org/10.2118/131094-MS.

Young LC, Stephenson RE. A generalized compositional approach for reservoir simulation. SPE J. 1983;23(05):727–42. https://doi.org/10.2118/10516-PA.

Zhao H, Lvov SN. Phase behavior of the CO_2–H_2O system at temperatures of 273–623 K and PRESSures of 0.1–200 MPa using Peng–Robinson–Stryjek–Vera equation of state with a modified Wong–Sandler mixing rule: an extension to the CO_2–CH_4–H_2O system. Fluid Phase Equilib. 2016;417:96–108. https://doi.org/10.1016/j.fluid.2016.02.027.